# 2

# METAL-CONTAINING POLYMERS: CRYOCHEMICAL SYNTHESIS, STRUCTURE, AND PHYSICOCHEMICAL PROPERTIES

L. I. Trakhtenberg and G. N. Gerasimov

*Karpov Institute of Physical Chemistry (Russian State Scientific Center), Moscow, Russia*

## 1. INTRODUCTION

Metal-containing polymers may be produced by various methods, such as chemical reactions of precursors—in particular, reactions of metal salts in polymer solutions, the treatment of polymers with metal vapors, or the polymerization of various metal–monomer systems [1–4]. Depending on the metal nature and the polymer structure, these processes lead to organometallic units incorporated into polymer chains, metal–polymer complexes, or metal clusters and nanoparticles physically connected with polymer matrix. Of special interest are syntheses with the use of metal vapors. In this case, metal atoms or clusters are not protected by complexones or solvate envelopes and consequently have specific high reactivity. It should be noted that the apparatus and principles of metal vapor synthesis techniques are closely related to many industrial processes with participation of atomic and molecular species [5]—for example, manufacturing devices for microelectronic from different metals and metal containing precursors [6]. Vapor synthesis methods employ varying metals and

*Metal-Polymer Nanocomposites*, Edited by Luigi Nicolais and Gianfranco Carotenuto
ISBN 0-471-47131-3 

organic ligands over a wide range. By such syntheses, one may prepare new organometallic compounds and complexes that are very difficult—and in, many cases, impossible—to synthesize by known methods [7].

Metal vapor techniques provide unique means for cryochemical solid-phase synthesis of metal-containing systems. In this way, metastable compounds, whose existence earlier was only supposed, have been obtained [7]. Besides, cryochemical processes produce stabilized small metal clusters of quantum type, which are the intermediate form of matter between isolated atoms and bulk metal [8, 9]. However, known methods of cryochemical solid-phase synthesis used low-molecular-weight matrices, in which the initial products of such a synthesis can be conserved only at low temperatures, when the matrix is enough rigid to hinder transformation or loss of these products.

In this connection, a cryochemical solid-phase synthesis of metal–polymer systems is of special importance. As a result of such a synthesis, metal clusters and organometallic assemblies formed at low temperatures are buried in a polymer environment, which offers possibilities to stabilize and study these products over a large temperature range. This method was first offered and described in reference 10. The thermal rearrangement of the initial low-temperature system is governed by relaxation processes in polymer matrix. In particular, the aggregation of metal atom clusters to form metal nanocrystals in cryochemically produced metal–polymer systems yields new nanocomposite materials with valuable properties. The study of the mechanism of cluster aggregation, which depends on the characteristics of the polymer matrix, will allow the nanocomposite structure to proceed in the needed direction. Thus, it becomes possible to determine the methods of cryochemical synthesis of metal–polymer materials with predetermined properties.

## 2. METHODS OF SOLID-PHASE CRYOCHEMICAL SYNTHESIS

Metal-containing polymers can be synthesized by the vapor deposition polymerization of various monomer systems including organometallic compounds and metal–monomer co-condensates. Such co-condensates are produced by simultaneous or layer-by-layer deposition of metal and monomer vapors on substrate plates at low temperatures (usually, 77 K). Polymerization can proceed in different ways. Some metal–monomer systems polymerize during co-condensation (Ge and Sn with acetylene [11], Mg with CN-substituted *p*-xylylene [12]), most probably due to heat released at condensation. In references 13–16, co-condensates of metals (Pd, Ag, Au, etc.) and vinyl monomers

prepared at 77 K were thawed, and thus the obtained metal colloids were polymerized in the liquid state under the action of radical initiators.

Such procedures gave composites only with very low metal concentration (0.01–1 wt. %) containing metal particles of rather large size (about 160 nm) [16]. Metal–polymer materials with high metal content can be prepared by polymerization of solid-vapor-deposited metal–monomer co-condensates. The first investigations in this field were carried out in 1959 for vitreous co-condensate of Mg-acrylonitrile, which polymerizes at softening of glass under action of active centers produced by electron transfer from Mg to acrylonitrile [17]. The state of metal in the obtained polymer system has been not characterized. Cryochemical synthesis is based on low-temperature solid-state polymerization in conditions of frozen molecular mobility in the reacting system. Earlier it was shown that a number of monomers, such as acrylonitrile [18], formaldehyde [19–21], or *p*-xylylene (PX) and its derivatives [22–24], polymerize in solid state under γ or UV radiation at 77 K and even close to the liquid helium temperature [18, 20]. It is suggested that such polymerization is caused by specific supramolecular organization of solid-monomer-containing molecular aggregates, which are precursors of polymer chains [25]. In such aggregates, mechanical perturbation arising during the radiation-induced chain generation under certain conditions can lead to the subsequent activationless growth of the polymer chain [26–28].

*p*-Xylylene compounds containing different substituents are the most suitable monomers for cryochemical synthesis of metal-containing polymers because they polymerize at low temperatures completely without the use of any foreign substances—in particular, initiators or sensitizers. By varying the substituents, one can modify physicochemical properties of the polymer matrix in the rather wide range. PX compounds arise by pyrolysis of corresponding [2,2]-*para*cyclophanes [29]. A scheme of preparation and polymerization of PX compounds is presented in Scheme 2.1.

The solid [2.2]-*p*-cyclophane was sublimated at 383 K, and the vapors were passed through a pyrolitic quartz tube at 873 K. This compound converts into PX without formation of detectable side products under these conditions [29, 30]. As stated in reference 22, solid PX most probably contains polymer chain precursors in the form of monomer stacks transforming into polymer chains as a result of the rather small rotational displacement of molecules without their translation movement. The assumed pattern of the solid-state PX polymerization is presented in Figure 2.1.

Metal-containing poly-*p*-xylylenes were synthesized from PX with organometallic substituents or from PX–metal co-condensates. In the latter case the PX vapors were mixed in the outlet of the pyrolytic tube with metal vapors produced by sublimation of the corresponding metal. Depending on the metal

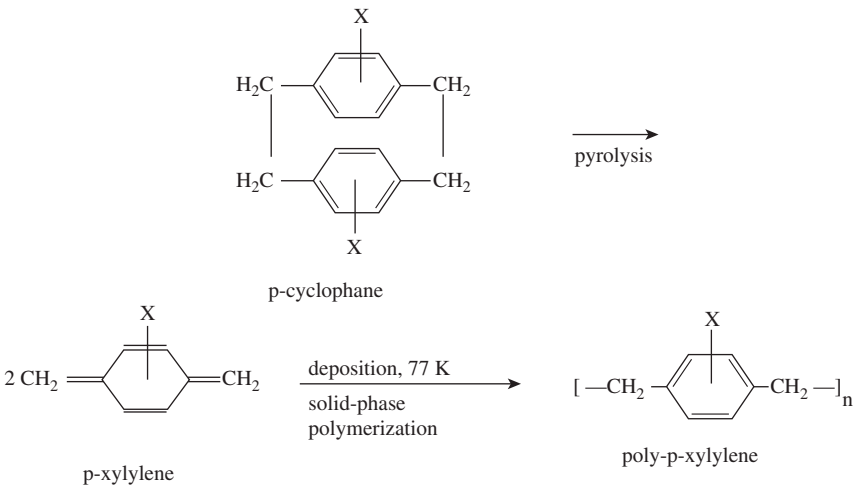


Scheme 2.1. Preparation and polymerization of *p*-xylylene monomers.

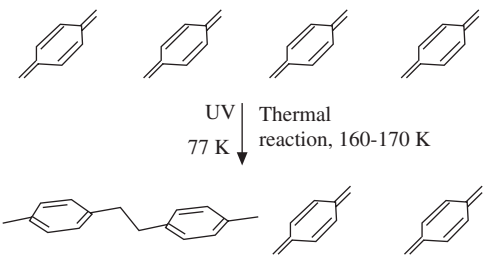


Figure 2.1. The assumed supramolecular structure of solid PX and the PX polymerization pattern.

volatility, such sublimation was performed by heating metal in a special tube supplied with a resistance heater or under the action of an electron (or ion) beam [30, 31]. The PX monomer alone or together with metal vapors was deposited onto a substrate plate, which was cooled to 77 K in an optical cryostat shown schematically in Figure 2.2.

Polymerization was induced by heating an obtained deposit or by its irradiation from a high-pressure mercury lamp. It has been shown that spontaneous thermal polymerization proceeds at temperatures close to 170 K [22], but under UV radiation PX polymerize completely even close to 77 K [21–23].

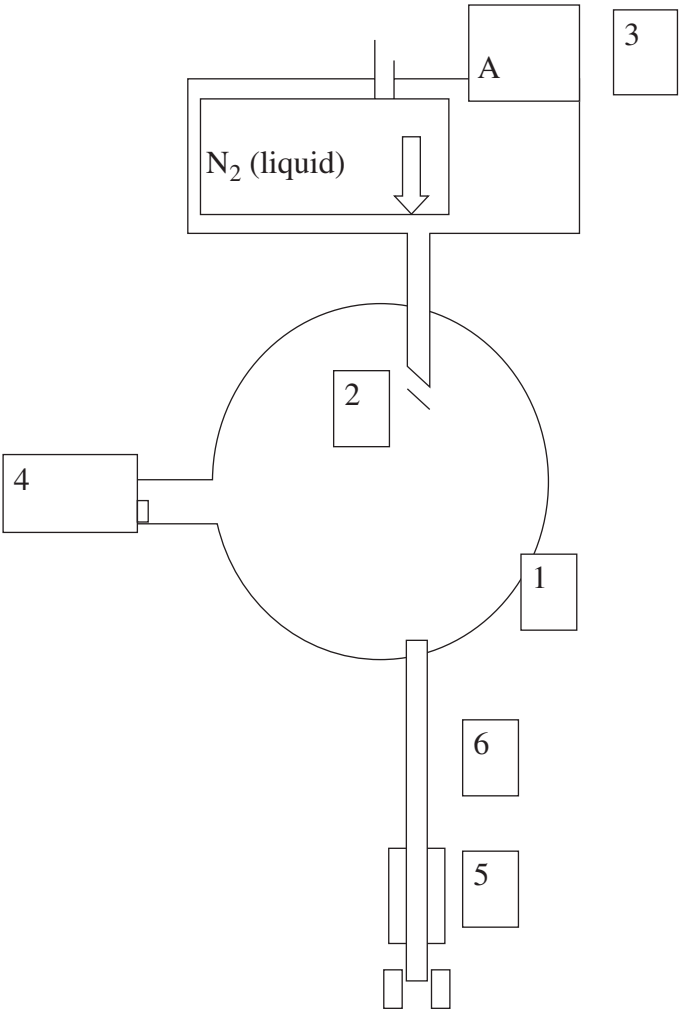


Figure 2.2. Schematic of apparatus for synthesis of a metal/SC-polymer nanocomposite: 1, vacuum chamber; 2, substrate holder; 3, resistance measurements (for metal control in the film); 4, heater (metal evaporation); 5, heater (cyclophane evaporation); 6, heater (cyclophane pyrolysis).

## 3. STRUCTURE OF CRYOCHEMICALLY SYNTHESIZED METAL–POLYMER COMPLEXES

Depending on the metal nature and monomer structure, the vapor deposition cryopolymerization of metal–monomer systems yields a possibility producing metal-containing polymers of different structure. Polymer containing organometallic groups or metal–polymer complexes can be prepared using pre-

liminary synthesized organometallic monomer or monomer and metal chemically interacting to one another during vapor co-deposition. In the later case, *p*-xylylene monomers are particularly attractive because of their high reactivity and ability to form complexes with metals due to low-lying π-orbitals. In the absence of chemical or coordination bonds between the metal and the monomer, the vapor deposition cryochemical synthesis gives metal clusters physically incorporated in a polymer matrix. The stability of low-temperature products of such a synthesis, as well as their transformation as a result of secondary thermal processes in matrix, depends on the structure and physicochemical properties of matrix.

## 3.1. Polymers Containing Organometallic Units

Organometallic derivatives of poly-*p*-xylylene (PPX) with Ge and Sn atoms covalently bonded to polymer chains have been synthesized by a vapor deposition technique using bridged [2,2]-*para*cyclophanes with corresponding organometallic groups [32, 33]. Pyrolysis of these cyclophanes, along with polymerization of the *p*-xylylene monomer mixture, is shown in Scheme 2.2.

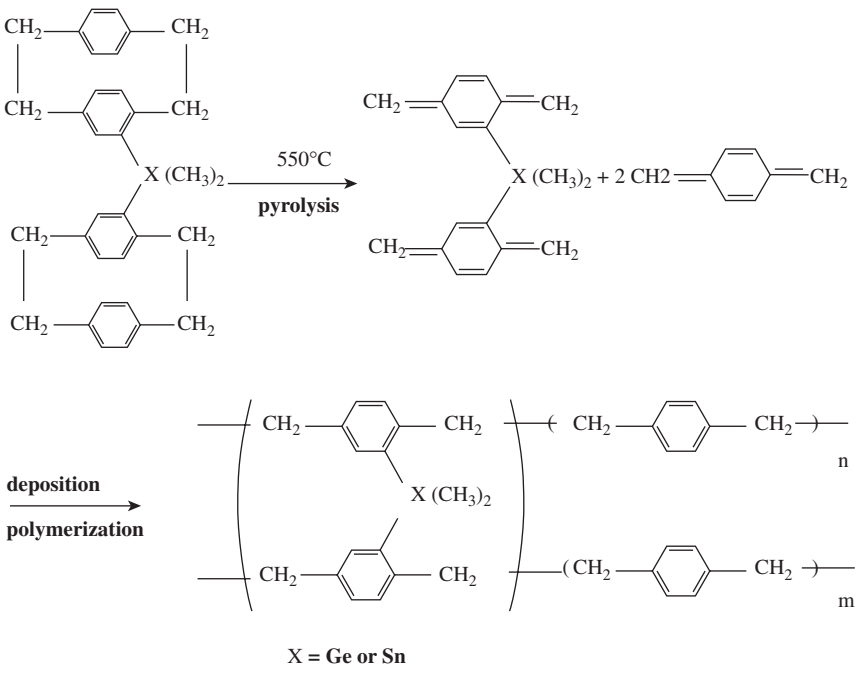


Scheme 2.2. Vapor-deposition preparation of poly-*p*-xylylenes containing organogermanium and organotin units.

It has been shown that the temperature of the deposition and polymerization of the monomer system strongly influences the structure of obtained polymers. Deposition of monomers at 77 K, followed by thermal low-temperature solid-state polymerization of the formed monomer composite, leads to crystalline block copolymers, whose structure, most probably, corresponds to that of microcrystalline monomer deposits. At the same time, deposition and polymerization of monomers at 283 K in conditions of high molecular mobility results in amorphous block copolymers or liquid-like oligomers [33]. The thermal decomposition of organotin units of corresponding crystalline copolymer in air yields $SnO_2$ microcrystals. Organogermanium blocks of the crystalline block copolymer decompose in an inert atmosphere, giving Ge microcrystals in a PPX matrix. Thermal treatment of amorphous block copolymers in the same conditions also leads to a total loss of Ge-organic structures, however, without formation of Ge crystals [33]. So, one can conclude that the supramolecular organization of the polymer produced by the cryochemical synthesis determines the direction of thermal decomposition of organometallic polymer fragments.

Polymers with organometallic units incorporated in a polymer structure can be also synthesized by the low-temperature solid-state polymerization of vapor deposited metal–monomer co-condensates, in which metal atoms or clusters form intermediate chemical or coordination bonds with monomer molecules and active centers of polymerization. As has been shown in reference 11, Ge and Sn atoms react with $C_2H_2$ during the deposition of metals together with a monomer at 77 K, producing acetylene–metal copolymers with composition $(C_2H_2{,}_7Ge_{0,72})_x$ and $(C_2H_2{,}_6Sn_{0,70})_x$. These metals (M) incorporated in polyacetylene structure are probably in the M(II) and M(IV) oxidation state. According to reference 11, the most probable structure of prepared copolymers can be presented by Scheme 2.3. These copolymers are weakly paramagnetic but lose

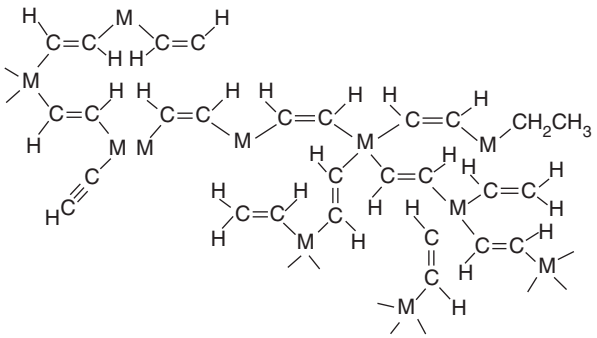

Scheme 2.3. The structure of polyacetylene containing chemically bounded Ge and Sn.

the paramagnetism as a result of their irreversible oxidation in $O_2$ with the formation of metal oxides [11].

The structure and polymerization of the vapor-deposited PX–Mg monomer system were described in references 23 and 34–37. Taking into consideration IR and UV–Vis spectral data, it was concluded that the co-condensation of Mg with PX at 77 does not lead to the PX polymerization but results in formation of charge transfer complexes where PX is in the benzenoid form [35, 36] (Scheme 2.4).

In the UV–Vis spectrum of this co-condensate, there is a very intense band with maximum close to 340 nm (Figure 2.3) [36]. This band lies between absorption bands of ionic organometallic compounds in the range 420–470 nm and those of organomagnesium derivatives with predominantly covalent Mg–C bonds in the range 280–300 nm [38, 39]. Thus, the bonds in complexes of PX with a magnesium atom (or cluster $Mg_n$) are neither purely ionic not covalent, but have intermediate structure. This was confirmed by quantum chemical calculations [36]. Polymerization under UV radiation at 77 K is accompanied by the shift of band from 340 to 310 nm (Figure 2.3), which means the transformation of initial complexes into organomagnesium units of PPX backbone chains [$–CH_2–C_6H_4–CH_2–Mg_n–$] with Mg–C bonds [35, 36] close to σ bonds of organomagnesium compounds. The fact that the absorbance maximum of Mg–C bonds in Mg–PPX is at 310 nm and not in the range 270–300 nm indicates some deformation of these bonds as compared to those of usual stable organomagnesium compounds. Initial monomer complexes are located in defects of monomer crystal between stacks shown in Figure 2.1 and do not sufficiently disturb the stack structure. The formation of organomagnesium units of PPX at low temperatures in conditions of frozen molecular mobility can be explained by the fact that the Mg–C bonds around $Mg_n$ are rather weak and are deformed in crystalline lattice to fit to polymer chain. The assumed pattern of the process is shown in Figure 2.4.

The stability of synthesized organomagnesium structures depends on atomic metal content $X_{at}$—that is, $N_M/N_M + N_P$, where $N_M$ and $N_P$ are the amount of metal atoms and polymer chain units, respectively. At high $X_{at}$ of Mg (>40

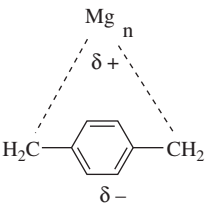


Scheme 2.4. The assumed structure of Mg–*p*-xylylene complex.

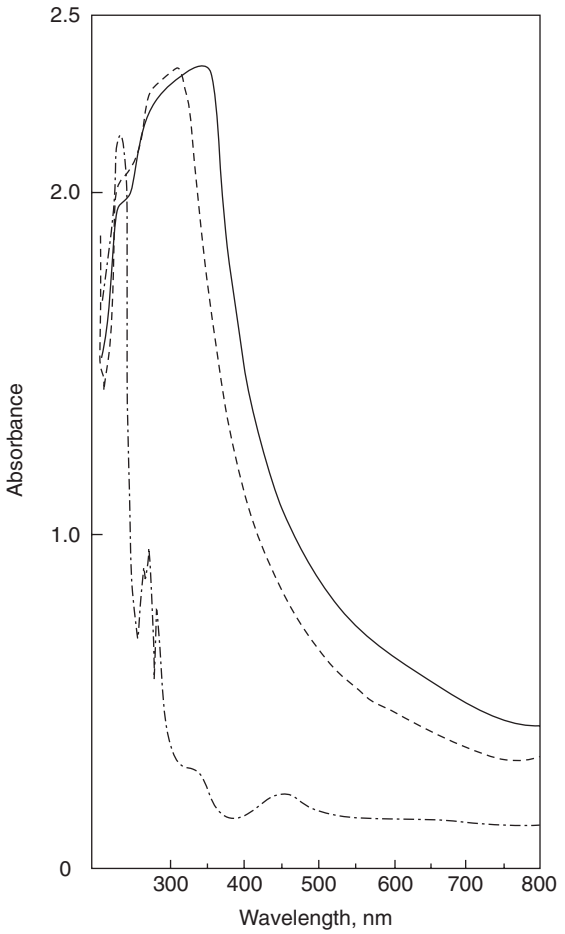


Figure 2.3. The UV–Vis spectra of the PX–Mg films with an Mg concentration of about 30 mol. %. Solid line, original co-condensate at 77 K; dashed line, after UV irradiation at 77 K (complete polymerization); dot–dashed line, after 36 hr of storage at room temperature in a vacuum.

at. %) these structures are stable in vacuum or inert atmosphere at room temperature and may be of interest as organomagnesium catalysts. Stability of obtained structures in this case is probably provided by the additional Mg–C bonds arising as a result of interaction between organomagnesium centers of PPX chains. This interaction leads to the formation of a tetrahedral configuration of Mg–C bonds that takes place in crystalline organomagnesium compounds [40, 41]. At $X_{at}$ of Mg $\leq$ 20 at. %, organomagnesium PPX units are destroyed at room temperature even in vacuum. In the spectrum of Mg–PPX

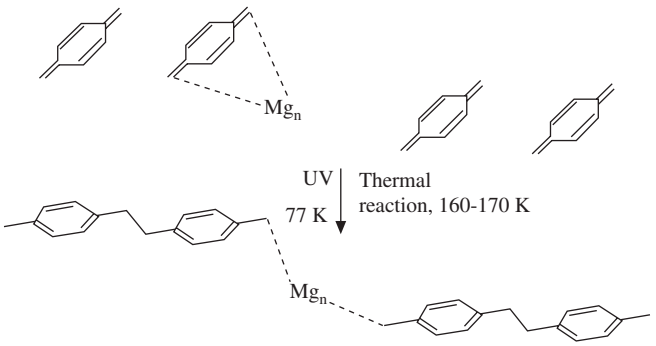


Figure 2.4. The assumed schematic pattern of producing organomagnesium PPX units during polymerization of a PX–Mg co-condensate.

annealed in vacuum at room temperature along with polymeric band, there are two new weak bands at 345 and 440 nm (Figure 2.3) that suggest the formation of $Mg_3$ clusters. Other Mg clusters, which probably form from organomagnesium structures, could not be observed on a background of PPX absorption [36]. In air at room temperature, organomagnesium structures and Mg clusters oxidize with the formation of MgO nanocrystals of mean size about 35 Å immobilized in PPX matrix [36].

The vapor deposition of PX with a C≡N substituent in the quinoid ring (CN-PX), together with Mg at 77 K, leads to polymerization of this monomer during deposition with the resulting formation of the corresponding substituted PPX (CNPPX) containing organomagnesium structures analogous to those in Mg-PPX [12]. But vapor co-deposition of Mg and CN–PX at 290 K accompanied by polymerization yields only CNPPX containing π complexes between Mg and nitrile groups of polymer [12]. The influence of the deposition temperature on polymer structure in this case was explained by the fact that the monomer polymerization and formation of intermediate Mg–monomer complexes differently depend on temperature. During low-temperature co-deposition the polymerization of the solid monomer phase proceeds rather slowly, and Mg incorporates into this phase before the monomer converts to polymer. At 290 K the rate of polymerization of deposited CN–PX is so high that Mg has no time to associate with a monomer and forms complexes only with C≡N substituents of polymer chains [12].

The co-condensation of Mn with PX at 77 K yields complexes of two types: charge transfer complexes analogous to those of Mg–PX and *d*-π complexes of quinoid PX involving *d* orbitals of Mn and π orbitals of PX [36, 42]. Polymerization at 77 K under irradiation is accompanied by the destruction of *d*–π complexes and transformation of charge transfer complexes to organoman-

ganese PPX units similar to organomagnesium ones [36, 42]. These units decompose at room temperature even in vacuum yielding clusters of Mn atoms. Clusters produced by the decomposition of organomanganese units and complexes form Mn nanocrystals in the interior of the PPX matrix. According to the data of TEM, the main crystal size is about 50 Å [36].

## 3.2. Polymers Containing Metal Clusters and Nanocrystals Physically Incorporated in Polymer Matrix

As was shown in the previous section, inclusions of zero-valent metal or inorganic metal compounds in polymer matrices (semiconductor compounds; in particular, metal oxides are of most interest, because the electron structure of semiconductor particles strongly depends on their size) can be prepared by the destruction of cryochemically synthesized organometallic polymer structures. However, in most cases metal does not interact chemically with a monomer, so that metal clusters and nanocrystals physically incorporated in polymer matrix are formed directly at vapor deposited cryochemical synthesis [4, 24, 43, 44]. The primary products of cryochemical syntheses involving such metals or semiconductors are small atomic or molecular clusters. When such a composite is warmed up, these particles combine into metal or semiconductor nanocrystals. The temperature range of this process depends on the structure of the polymeric matrix. The stabilizing properties of the matrix can be enhanced to the extent that small atomic and molecular clusters remain intact in this matrix for a long time even at room temperature. This can be done by varying substituents in PPX polymer chains.

The metal particles, both clusters and nanocrystals, in the composite films are stabilized without any specific coordination bonds between the particulate surface and the polymer environment or without any special stabilizing compounds. The particles have only weak (Coulomb and van der Waals) interaction with the environment, and their size is due mainly to the stiffness of the matrix, in the interior of which the particles are formed. This is the primary advantage of the cryochemical solid-state technique over other conventional methods. The technique allows growth of particles over a wide size range, including small clusters, in nonpolar as well as hydrophobic polymer matrices. The concentration of nanoparticles can also vary widely up to high values, providing useful properties resulting from their interaction. The structure and properties of nanocomposites are determined by the fraction of volume occupied by metal particles that is volume content of metal $X_V$. Therefore, this parameter is mainly used further at the description of composites. It relates to above-defined atomic content $X_{at}$ as $X_V = \rho_P X_{at}/[\rho_P X_{at} + \rho_M(1 - X_{at})M_P/M_M]$, where $\rho_P$ and $\rho_M$ are the density of polymer and metal, respectively, and $M_P$ is the molecular weight of the polymer chain unit and $M_M$ is the atomic weight of the metal. The

vapor-deposited low-temperature synthesis allows preparing composites with $X_V$ up to 50%.

Co-condensation of gold vapor and the diacetylene monomer at 77 K followed by warming up the condensate gave a polymer with conjugate π bonds, which contained gold nanoclusters and had unusual optical properties [45]. Metal–polymer composites prepared by thermal polymerization of low-temperature co-condensates of acrylic acid or methyl acrylate with some metals were described in reference 46. Polymer composites contained metal particles of size in the range 5–15 nm.

Cryochemical synthesis of Ag–PPX systems and their structures were studied in references 24, 34, 36, 37, and 44. The simultaneous vapor deposition of PX-, CN–PX-, and Cl-substituted PX (Cl–PX) with Ag at 77 K does not lead to complexation or the formation of any organometallic compounds [24, 36, 44]. In the case of PX and Cl–PX, such deposition proceeds without polymerization. The co-deposition of CN–PX with Ag is accompanied by the partial polymerization of monomer. The initial condensates at 77 K contain a small amount of Ag nanocrystals that can be revealed and characterized using UV–Vis spectroscopy because such crystals have the specific absorption band of surface electron plasmons of about 430 nm [3] (Figure 2.5 and 2.6). UV irradiation of these condensates at 77 K leads to the total conversion of monomers to the corresponding polymers (PPX, ClPPX, and CNPPX). However, intensity ($D_{cr}$), maximum position ($\lambda_{max}$), and half-width ($\Delta_{1/2}$) of the nanocrystals plasmon band do not practically change in the course of cryopolymerization (Figures 2.5 and 2.6, Table 2.1).

Because $D_{cr}$ is proportional to the content of Ag nanocrystals and $\Delta_{1/2}$ is in inverse proportion to their mean size ($\bar{\mathbf{d}}$) [3, 47], one may conclude that the state and amount of Ag nanocrystals were not affected by the cryopolymerization [24, 36, 44]. Sharp growth of $D_{cr}$ at heating of obtained metal–polymer films specifies that the main part of Ag at 77 K is in a form of small noncrystalline $Ag_n$ clusters, which aggregate with formation of nanocrystals under the action of thermal relaxation processes in the polymer matrix. In UV–Vis spectra of PPX films on a background of the PPX absorption, it is possible to observe only absorption bands of $Ag_n$ with $n > 15$, which, according to reference 9, should be in an "open" range of PPX spectrum at $\lambda > 320$ nm. Because in this spectral range there are no absorption bands except for the absorption band of Ag nanocrystals, it may be concluded that clusters stabilized in obtained films contain less than 15 atoms [24, 44].

A solid polymer matrix hinders the aggregation of cryochemically prepared Ag clusters so that substantial part of Ag in the prepared Ag–PPX systems remains in noncrystalline form at ambient and even higher temperatures. As was stated in references 24, 36, and 44, all of the Ag introduced into the investigated PPX matrices transforms to nanocrystals after annealing at 373 K.

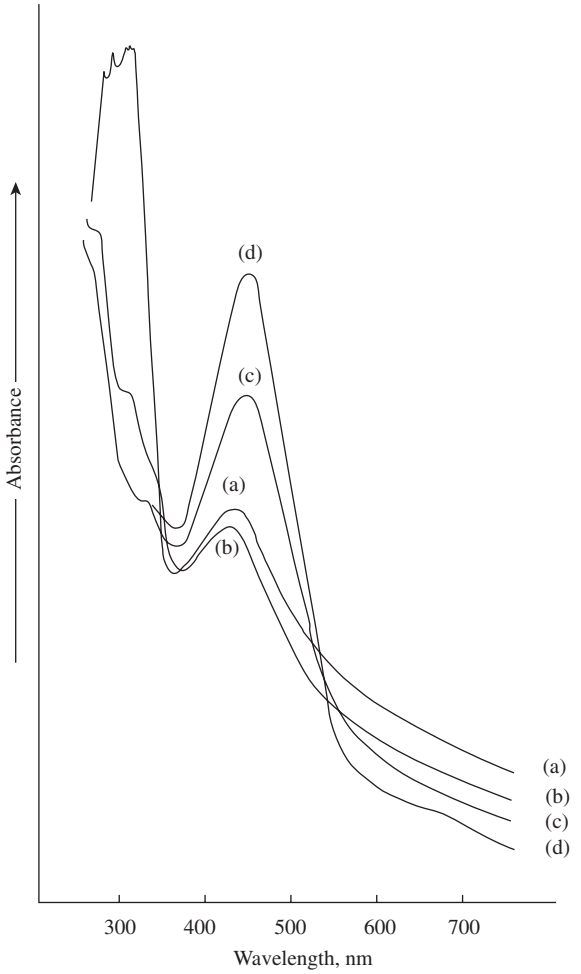


Figure 2.5. The UV–Vis spectra of solid films at 80 K: (**a**) Films obtained by co-condensation of Ag and ClPX at 80 K; (**b**) the same films polymerized under UV irradiation at 80 K; polymerized films after annealing at (**c**) 293 K and (**d**) 373 K.

Therefore the ratio of $D_{cr}$ in a spectrum of an examined film to $(D_{cr})_0$ in a spectrum of the same film annealed at 373 K characterizes a degree of the cluster crystallization (Table 2.1). Spectral data show that the position of plasmon band for nanocrystals in Ag–PPX films heated from 77 to 298 K shifts to the long-wavelength range and then does not change at heating from 298 to 373 K (Table 1). The same effect was observed for Ag–ClPPX films [24].

It should be noted that, unlike Ag nanocrystals of Ag–PPX nanocomposites with $\lambda_{max}$ of a plasmon band in the range 430–445 nm, nanocrystals

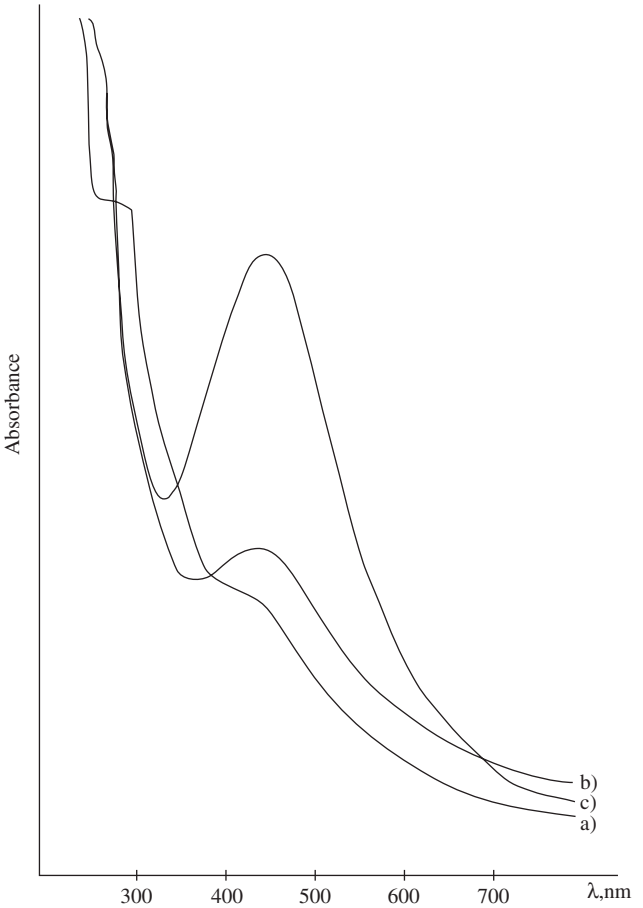


Figure 2.6. The UV–Vis spectra of solid films at 80 K: (**a**) Films obtained by co-condensation of Ag and CNPX at 80 K; (**b**) the same films polymerized under UV irradiation at 80 K and annealed at 293 K; (**c**) polymerized films after annealing at 373 K.

TABLE 2.1. Spectral Characteristics and Content of Ag Nanocrystals in the Solid System During the Synthesis of an Ag–PPX Nanocomposite

| System | $\lambda_{max}$ (nm)[a] | $\Delta_{1/2}$ (nm)[a] | $D_{cr}$ (at $\lambda_{max}$)[a] | Content of Ag Nanocrystals (at. %) |
|---|---|---|---|---|
| PX–Ag at 77 K | 430 | 93 | 0.24 | 4.2 |
| PPX–Ag at 77 K | 430 | 93 | 0.24 | 4.2 |
| PPX–Ag at 298 K | 435 | 96 | 0.28 | 5.0 |
| PPX–Ag at 320 K | 443 | 98 | 1.10 | 16.3 |
| PPX–Ag at 373 K | 443 | 98 | 1.22 | 18.0 |

[a] Designations are supplied in the text (see above).

prepared by reduction of $Ag^+$ ions in solution of poly (*N*-vinylpyrrolidone) and protected by molecules of this polymer have a plasmon band with $\lambda_{max}$ at 410 nm [48]. As is specified in reference 48, the UV–Vis spectrum of nanocrystals depends on their size and form as well as on the embedding matrix. The plasmon band of Ag nanocrystals in reference 48 coincides with that of modeling spherical nanoparticles with a smooth ideal surface, which were theoretically treated from different points of view in references 49 and 50. The nanocrystals of this type form in various liquid media, such as organic solution [3, 48] or the softened quasi-liquid glass [49, 50], where there are no steric hindrances for the growth of equilibrium crystals without surface defects. At the same time, barriers for aggregation of clusters or atoms to metal nanocrystals in the solid system that arises during the cryochemical solid-state synthesis favor the formation of crystals with structural defects, especially on the crystal surface. This increases the surface diffuseness of such nanocrystals resulting in the red wavelength shift of the surface plasmon resonance [51]. The defreezing of the polymer matrix and corresponding alteration of the metal–dielectric interface can explain the further increase of $\lambda_{max}$ of the plasmon band.

The cluster aggregation to nanocrystals depends on the metal content. In the obtained Ag–ClPPX films the relative part of metal, stabilized in cluster form at 293 K, decreases from 90% to 20% while increasing the total metal content from 0.25 to 2 vol. % [44]. The stability of clusters is greatly influenced also by the structure of the polymer matrix [36, 44]. Comparison of spectra in Figures 2.5 and 2.6 shows that in cryochemically synthesized films, the Ag–CNPPX stability of Ag clusters is much higher than that in similar films Ag–ClPPX. The data on $D_{cr}/(D_{cr})_0$ (see above) in the spectra of various films show that in cryochemically synthesized Ag–CNPPX films heated to ambient temperature, up to 70% from total incorporated Ag (in amount of about 2 vol. %) is stabilized as small noncrystalline clusters [44]. A similar result has been reported in reference 36 for Ag–PPX (Table 2.1). But in Ag–Cl–PPX containing the same total Ag, the fraction of Ag clusters at 295 K is only about 20% [24, 44].

The rather high stability of Ag clusters in Ag-containing PPX can be explained by features of the PPX amorphous phase where clusters are mainly localized. Due to the absence of substituents in PPX chains, this phase differs probably from a similar phase of substituted PPX in higher density and consequently hinders the cluster aggregation in the greater degree. In CNPPX (as compared with ClPPX) there is probably the specific interaction between electron-donating Ag clusters and electrophilic CN groups of the polymer environment that provides a high stability of clusters.

The $\bar{\mathbf{d}}$ value estimated from $\Delta_{1/2}$ of the nanocrystal surface plasmon band in spectra of Ag–ClPPX is about 45 Å [44]. Spectral data for cryochemically

prepared Ag–PPX [36] testify to the fact that $\bar{\mathbf{d}}$ is much the same. The calculation based on $\Delta_{1/2}$ of the 110-reflection peak of Ag nanocrystals in an X-ray diffractogram of Ag–ClPPX film gave a $\bar{\mathbf{d}}$ value close to 50 Å [24] (Figure 2.7). The diffractogram of a model system obtained by layer-by-layer deposition of a ClPX monomer and Ag at 77 K, followed by photoinduced polymerization at the same temperature and annealing at 293 K, is also shown in Figure 2.7. Although the interfacial energy on the boundary Ag–polymer matrix in the layered system and the polymerized co-condensate is the same, the value of $\bar{\mathbf{d}}$ in the layered system is approximately equal to 120 Å [24]. So $\bar{\mathbf{d}}$ of Ag nanocrystals in a co-condensate is determined mainly by steric restrictions on the crystal growth in the interior of solid matrix.

The Ag-containing PPX was investigated by TEM. The TEM pattern demonstrates globular particles of sizes between 20 and 120 Å quite homogeneously dispersed within the polymeric matrix [36]. Histogram of the particle size distribution (Figure 2.8) shows that the main particle size is between 40 and 60 Å, which is in good agreement with the results of X-ray and spectral measurements for Ag–ClPPX. Similar histograms were determined by TEM for Pb- (Figure 2.9), Zn-, and Cd-containing nanocomposite PPX films prepared

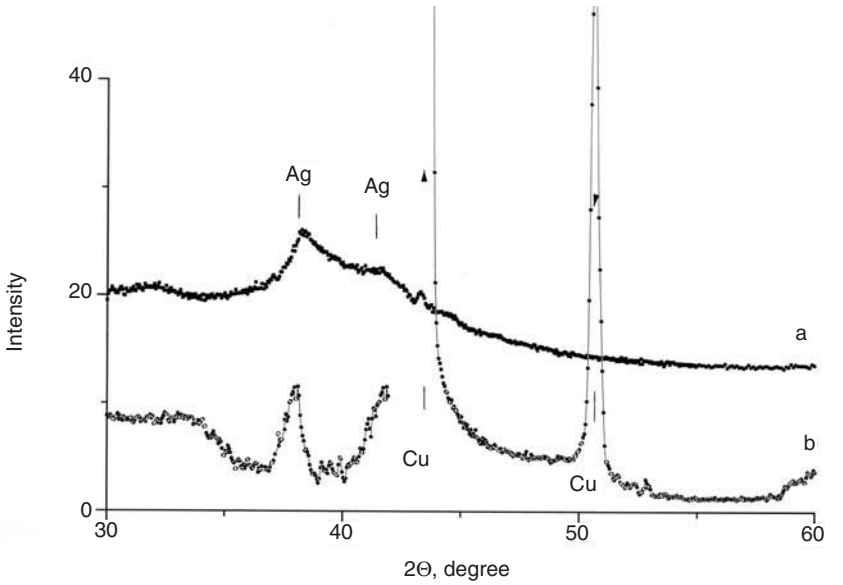


Figure 2.7. X-ray diffractograms of Ag–poly(chloro-*p*-xylylene) systems: (**a**) co-condensate Ag–C1PX polymerized at 80 K and annealed at 293 K; (**b**) layer-by-layer deposition of C1PX and Ag followed by polymerization and annealing at 293 K. X-ray diffractogram peaks of Cu foil are used as a standard.

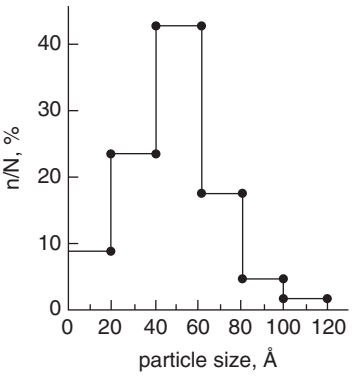


Figure 2.8. Histogram of the size distribution for PPX–Ag films.

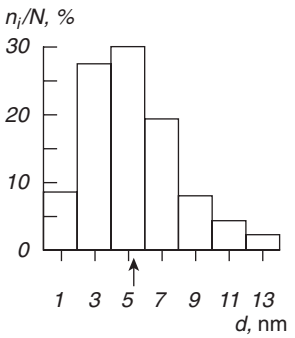


Figure 2.9. Histogram of the size distribution for PPX–Pb films. Arrow shows the mean size of Pb nanocrystals.

by vapor deposition cryochemical synthesis [52]. The value $\bar{\mathbf{d}}$ of metal nanocrystals in these films is about 50 Å. Approximately the same size $\bar{\mathbf{d}}$ (about 45 Å) has been evaluated from $\Delta_{1/2}$ of X-ray diffraction peak for semiconductor PbS nanocrystals in PbS–PPX nanocomposite prepared by the vapor deposition of PX together with PbS at 77 K followed by heating of obtained monomer system to 293 K [53].

So, the mean size of metal or semiconductor crystals in cryochemically prepared PPX nanocomposites depends almost not at all on the nature of such crystals but is determined by the polymer matrix. In particular, data on the width of the nanocrystals plasmon band [44] (cf. Figures 2.5 and 2.6) specify that $\bar{\mathbf{d}}$ of nanocrystals formed from Ag clusters in CNPPX is, approximately, in one and a halftime less than that of analogous nanocrystals in PPX and ClPPX.

Based on spectral data, it has been concluded that the change of Ag content in the cryochemically synthesized films Ag–PPX and Ag ClPPX from 0.3 to 2 vol. % (that is, 4–20 at. %) does not influence $\bar{\mathbf{d}}$ of Ag nanocrystals formed as a result of the cluster aggregation [36, 44]. The same result has been obtained for Pb–PPX films with Pb content varied from 0.01 to 1 vol. % [52]. Unlike other similar systems, PbS–PPX nanocomposites were studied at high PbS loading in the range from 4.7 to 10.2 vol. % of PbS. In this case according to X-ray data, $\bar{\mathbf{d}}$ of PbS nanocrystals also does not depend on PbS content [53]. Thus, it may be concluded that the independence of the nanocrystal mean size from the metal or semiconductor content is a general feature of nanocomposites resulted from solid-state synthesis.

The growth of nanoparticles in a polymerized system has been considered in reference 54. This process was modeled by assuming instantaneous nucleation followed by deposition of metal atoms on the surface of growing nucleus due to diffusion of atoms incorporated in polymer to the nucleus. At modeling it was taken into account that in a polymerized system the diffusion coefficient of metal atoms strongly decreases with an increase in conversion of monomer to polymer in relation to a decrease of free volume of the system during polymerization [54]. The model allows establishing the dimensionless parameters that determine the formation of nanocomposite films and their structure during classical polymerization processes [55]. But at the solid state, cryochemical synthesis processes of polymerization and formation of nanocrystals occur separately: During low-temperature polymerization the aggregation of metal atoms and small metal clusters is frozen and proceeds after polymerization at heating of obtained polymer system.

The polymer structure resulting from the low-temperature solid-state polymerization corresponds to the structure of solid microheterogeneous monomer deposit and contains deep and shallow traps. It is possible to assume that growing crystal nuclei are formed from metal clusters immobilized in deep traps. Metal atoms and clusters situated in shallow traps are released as a result of thermal relaxation processes and join with growing nuclei. The relationship between deep and shallow traps is governed by polymer composite morphology and properties. In this case the concentration of nuclei is proportional to metal content and thus the mean size of nanocrystals; that is, the mean amount of metal per nucleus does not depend on metal content. From this point of view, the fact that crystallization in CNPPX produces Ag nanocrystals smaller than those formed in other PPX matrices can be explained by an increase of the relative part of specific deep traps for Ag clusters in a polymer matrix with electron-accepting CN groups. This leads to an increase of the relative part of crystalline nuclei in the total amount of Ag clusters and, as a consequence, leads to reduction of the mean size of nanocrystals.

Properties of a polymer composite containing metal or semiconductor nanocrystals depend not only on the mean size of nanocrystals, but also on their size distribution. The dependence of the crystallite size distribution on PbS content was investigated for cryochemically synthesized nanocomposite PbS–PPX films in the range from 4.7 to 10.2 vol. % of PbS. The distribution curves obtained from analysis of wide-angle X-ray scattering (WAXS) data is presented in Figure 2.10 [53, 56, 57]. As can be seen, the distribution is not very broad, extending from 20 to 150 Å; the main population of PbS crystallites has a size much less than 100 Å. The curve for nanocomposites with 4.7 vol. % of PbS is similar to histograms of the crystallite size distribution determined by TEM for nanocomposite films Ag–PPX and Pb–PPX with low metal content (Figures 2.8 and 2.9). It means that, as well as the average size of crystals, distribution of the sizes does not depend on the nature of the metal or semiconductor incorporated in a polymer as a result of cryochemical synthesis. The few exceptions are the systems distinguished by specific interaction between metal clusters, which are precursors of nanocrystals, and polymers, as, for example, the system Ag–CNPPX (see above).

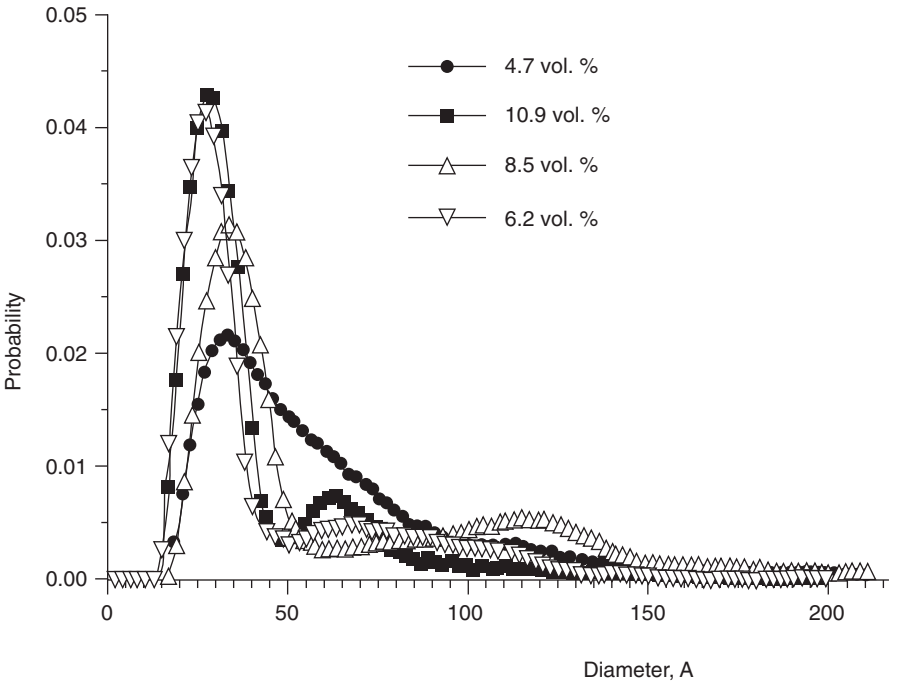


Figure 2.10. Size distribution of PbS crystallites versus PbS concentration in the PPX–PbS composite.

A PbS–PPX nanocomposite with 4.7 vol. % of PbS was investigated also by the small-angle X-ray scattering (SAXS) method, which characterizes different PbS inclusions in PPX matrix regardless of their internal structure. The size distribution of PbS inclusions calculated from SAXS data is similar to the WAXS crystallite size distribution on Figure 2.10. This result signifies that PbS nanoparticles do not aggregate in matrix but are distributed in PPX mostly as small crystallites [53].

It has been shown that the arrangement of nanocrystals in composite films is determined by the PPX supramolecular structure. The SAXS curve at relatively small PbS content of 4.7 vol. % has a broad maximum (Figure 2.11), which specifies some order in an arrangement of PbS nanocrystals. In this case, the PPX matrix retains its semicrystalline structure [53]. In such a matrix the nucleation and subsequent growth of inorganic nanocrystals takes place mostly in amorphous regions where there is enough free volume. It is possible that the observed SAXS maximum corresponds to an average periodicity between PbS nanocrystal assemblies in different amorphous regions separated by PPX lamellar crystallites. The characteristic parameter of this supramolecular periodicity is about 250 Å, which approximately coincides with thickness of PPX lamellas [53].

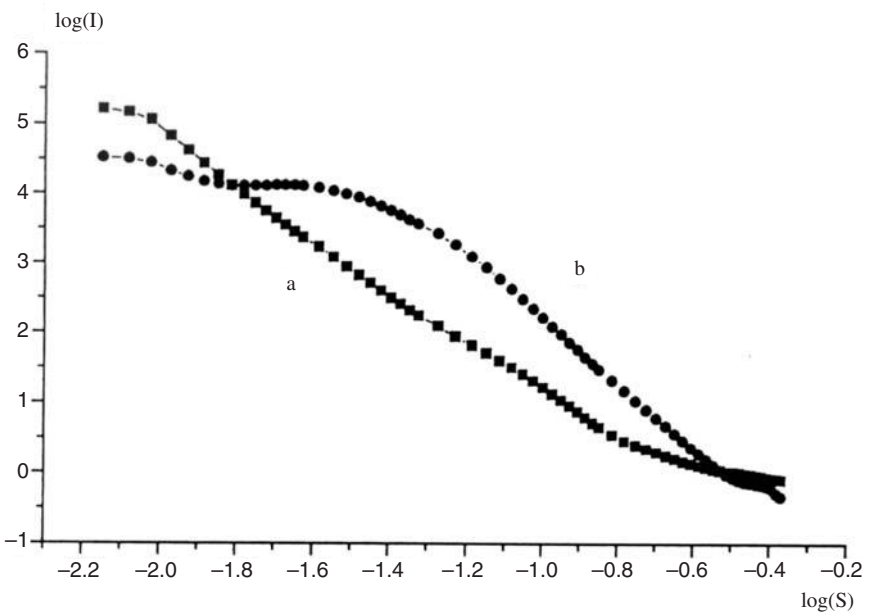


Figure 2.11. Small-angle X-ray scattering of PPX–PbS composite film with 4.7 vol. % of PbS (**b**) and of pure PPX film (**a**).

An increase in the concentration of PbS leads to the change of the crystal size distribution, which acquires a bimodal form. Recently, it was shown that this type of bimodal crystal size distribution takes place not only in PPX–PbS samples, but also in PPX-containing Ag nanocrystals [58]. Unlike other analogous systems, the composites obtained by the cryochemical solid-state synthesis demonstrate a marked increase in the percentage of small crystals with increasing content of inorganic component (metal or semiconductor) incorporated in a polymer. Figure 2.10 shows that the contribution of PbS crystallites of approximately 30-Å size increases from 20% to 80% with an increase in the overall PbS content from 4.7 to 10 vol. %. At the same time, the high PbS loading favors the formation of rather large crystals in the 70-Å size range. For this reason the crystal mean size determined from the half-width of the X-ray diffraction line does not change significantly and remains in the range 40–50 Å.

The reasons for such an unusual change of the crystal size distribution curve with increasing metal content are not precise investigated now. Preliminary data show [56] that an increase in the content of metal or semiconductor inclusions decreases the polymer matrix crystallinity and polymer crystal size. It is believed that this process is accompanied by the formation of a large number of local defect sites where the introduced inorganic component nucleates in the polymer matrix. The nucleation at high inorganic loading increases the rigidity of a system, which retards the crystal growth associated with the reorganization of system and redistribution of free volume. Therefore, the main part of crystals has a small size. At the same, time an increase in metal (or semiconductor) content can lead to formation of spatial defects with high free volume where nanocrystals have the ability to coagulate, giving rather large crystalline clusters. It may be supposed that such defects arise under strains accompanying nucleation at high loading.

## 4. PHYSICOCHEMICAL PROPERTIES OF SYNTHESIZED METAL–POLYMER FILM MATERIALS

Vapor-deposition solid-state synthesis can produce composites with high (close to percolation threshold) content of stable metal particles of varying size, trapped inside different polymer matrices. Due to the high metal content obtained, nanocomposites possess important valuable properties. First, the effects caused by the local behavior of isolated particles are sharply amplified (for example, the density of magnetic data recording in composite containing ferromagnetic monodomain nanoparticles). Furthermore, in nanocomposites with high metal content, one should take into account the interaction between nanoparticles, which determines cooperative behavior of the system of metal nanoparticles immobilized in polymer matrix. This interaction manifests itself

mainly as charge transfer processes between nanoparticles [59]. In particular, these processes substantially influence electrophysical and dielectric properties as well as catalytic activity of metal–polymer materials synthesized by the vapor deposition technique.

## 4.1. Conductivity and Photoconductivity

Metal–polymer systems obtained as a result of vapor deposition cryochemical synthesis contain stabilized small nonmetallic clusters of metal atoms and metal nanocrystals, but only metal nanocrystals participate in conductivity processes. The data on Ag-containing PPX composites [44] testify to the fact that the relative part of metal stabilized in cluster form at ambient temperature sharply decreases with increasing total metal content even in the range 0–2 vol. %. Therefore, at measurements of conductivity, which were carried out at considerably higher metal concentrations, it was accepted that as a first approximation, all metal is as nanocrystals.

When metal particles are isolated in a polymer so that the interaction between them can be neglected, the conductivity of a composite is determined by that of a polymer matrix. In such composites, metal nanoparticles can only inject carriers into a polymer but do not influence substantially the conductivity process [59]. This is the case of metal–PPX films prepared by the cryochemical vapor deposition technique if such films contain metal or semiconductor nanocrystals in amounts less than 4–5 vol. % [30]. The conductivity of such composites follows classical ohmic current–voltage relationship [30] and Arrhenius dependence on temperature [57]. At higher metal contents the mechanism of conductivity in synthesized composite films changes under influence of the interparticle interaction. In PPX films containing Pb nanoparticles in amounts from 5 to 10 vol. %, the dependence of current $I$ on voltage $U$ looks like $\ln I \sim U^{1/2}$ [30]. This dependence is characteristic for a current caused by the tunnel electron transfer between nanoparticles [60]. As is stated in reference 59, the tunnel current arises because at the certain metal content the nanoparticles participating in processes of tunnel electron transfer form infinite cluster penetrating all sample of a composite (percolation threshold). The barrier for the interparticle electron transfer decreases with increase in number of particles in infinite cluster and corresponding reduction of distances between them. As a consequence, probably, the $I$–$U$ relationship of the conductivity in synthesized Pb–PPX nanocomposites returns to the ohmic one at the rise of Pb content above 10 vol. % [30]. The percolation transition to tunnel conductivity precedes the transition to metalic conductivity resulted from direct contacts between metal nanoparticles. In PPX films containing Ag nanocrystals the conductivity is of metal type at metal content about 7 vol. %: conductivity of composite increases with lowering temperature proportional to

$(1 + \alpha T)^{-1}$ as that of block metals, but coefficient $\alpha$ is approximately in 2.5 times less than value $\alpha_0$, characteristic for block silver [57].

PPX composite films containing semiconductor nanocrystals of PbO (formed by oxidation of Pb nanocrystals) and PbS show photoconductivity [30, 53]. In the PbO–PPX films the photocurrent value ($I_{ph}$) in the wavelength range 250–350 nm does not depend on wavelength, and the ratio between $I_{ph}$ and dark current is close to $10^4$. Then $I_{ph}$ is gradually reduced up to zero at an increase of wavelength to 450 nm [30].

In the PPX films containing semiconductor PbS nanocrystals of mean size about 45 Å, the photoconductivity has been found even at 630 nm. This wavelength is close to the long-wave edge of the electron absorption of nanocrystals determined from UV–Vis of the films [53]. $I_{ph}$ in PbS–PPX is proportional to the 0.8–1 power of the light intensity, and the activation energy of photoconductivity is $10^{-1}$–$10^{-2}$ eV. The energy of light quantum at wavelength 630 nm is about 2 eV, whereas the electronic work function of PbS nanocrystal is higher than 4 eV. This circumstance has led to a conclusion that observed photoconductivity is caused by the photoinduced tunnel electron transfer [53]. The conclusion proves to be true by the low value of the activation energy of photoconductivity and by the nonlinear voltage dependence of photocurrent, which follows the relation $\ln(I_{ph}) \sim U^{1/2}$ characterizing tunnel current (see above). The photocurrent response time is 0.2–0.5 sec [53]. Such a high (for the electron photo detachment) value of the response time suggests that photocurrent proceeds with participation of intermediate long-lived electron–hole pairs generated by light in semiconductor nanocrystals and localized presumably on their defects [cf. reference 61].

## 4.2. Sensor Properties

Cryochemically synthesized PPX films containing metal or semiconductor nanocrystals have a fine porous structure caused by features of solid-state polymerization. Due to this structure, molecules of gaseous substances readily penetrate into polymer film from the environment. Synthesized composite films demonstrate valuable strong sensor effects resulting from a marked influence of some low-molecular-weight molecules, diffusing into the polymer and adsorbed onto nanocrystals, on the film conductivity [4, 30, 62–64]. Such effects are characteristic of films whose conductivity is governed by electron transfer between nanoparticles.

PPX films containing PbO nanocrystals are sensitive sensors on humidity. The conductivity of the PPX film with about 10 vol. % of PbO nanocrystals versus the air humidity is presented in Figure 2.12. PbO nanocrystals in a PPX matrix are formed by oxidation of Pb nanocrystals in Pb–PPX nanocomposite films produced by cryochemical synthesis (see above).

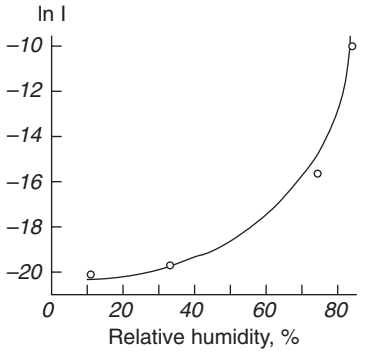


Figure 2.12. Current *I* (in amperes) in PPX–PbO films versus air humidity.

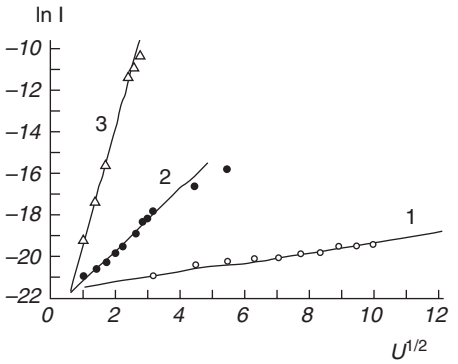


Figure 2.13. Current *I* (in amperes)–voltage *U* (in volts) relationship for PPX–PbO films at various air humidity levels: 1, 11%; 2, 75%; 3, 85%.

It is believed that the adsorption of water molecules on the boundary between the semiconductor PbO and the PPX matrix gives localized ionic states that lead to the lowering of the barrier for the interparticle electron transfer [65]. The current–voltage relationship at various values of air humidity (Figure 2.13) testifies to the tunneling mechanism of the conductivity [30]. The complex character of the conductivity dependence on humidity in Figure 2.12 can be explained by the nonlinear dependence of the tunneling barrier on the amount of water adsorbed on nanoparticles. The influence of air humidity on the film conductivity is reversible: After the replacement of humid air with dry air, the conductivity comes back quickly to an initial value for dry air (Figure 2.14). As seen from Figure 2.14, direct and reverse response times are about 10–15 sec.

It should be noted that the essential rise of conductivity under water vapors has been observed in reference 59 for the composite CuS–polyvinyl alcohol

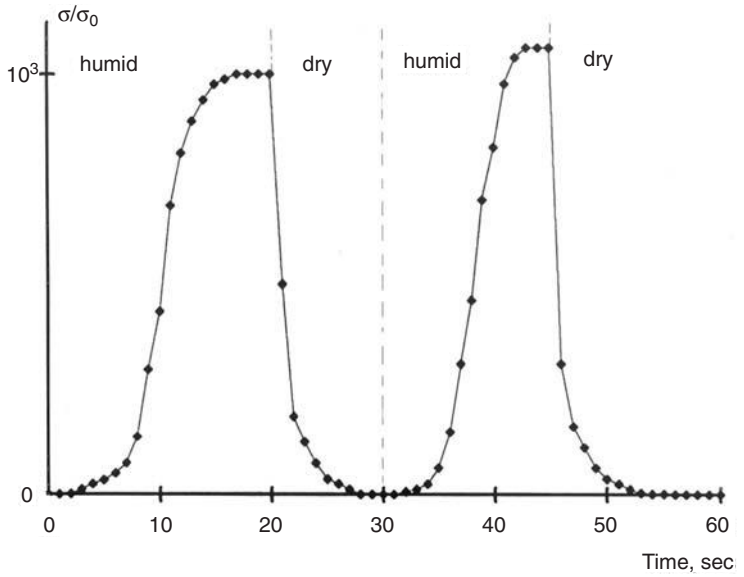


Figure 2.14. Film conductivity σ variations in response to repeated replacement of dry air by humid air, and vice versa. $\sigma_o$ is film conductivity in dry air.

film obtained by the classical liquid-phase method and contained semiconductor CuS nanocrystals. The effect has been explained by the fact that the absorption of water vapors increases the polymer permittivity, resulting in an increase of the electron tunneling probability between nanoparticles [59]. In this case the model is in rather good accordance with experimental data because polyvinyl alcohol is a hydrophilic polymer and absorbed water is dissolved and distributed evenly in polymeric matrix. Therefore, macroscopic characteristics of a polymer environment can be used for the description of the effect of water. But this model is not applicable to nanocomposite films based on hydrophobic PPX, where molecules of water "are pushed out" from the polymer and located on semiconductor particles. Such films are much more influenced by atmospheric water than are similar composite films based on the hydrophilic polymer in reference 9.

PPX films containing PbO nanocrystals show also a strong increase in their conductivity under the action of small quantities of ammonia and ethanol vapors in gaseous environment [30, 62, 63]. The effect from ammonia was observed in films with 5 vol. % of PbO. It is believed that the adsorption of ammonia lowers barriers for the electron transfer to a greater degree than that of water, which is why the sensitivity to ammonia appears at a lower concentration of semiconductor particles. The increase of conductivity of PbO–PPX nanocom-

posite films under ethanol vapors was revealed at PbO content about 15 vol. % [63]. Apparently, ethanol adsorbed on PbO influences the barrier of electron transfer between nanoparticles less than water and ammonia. The responses of conductivity to ammonia and ethanol are also reversible: The film conductivity returns to its initial value after the removal of these substances from the surrounding atmosphere.

Sensor response to low hydrogen pressures at ambient temperature for the PPX film containing Pd nanocrystals is presented in Figure 2.15 [64]. The electrical resistance of the film increases under the influence of hydrogen, presumably because of dissociative adsorption of hydrogen molecules on Pd nanocrystals that leads to the rise of the electron work function of these nanocrystals [66] and correspondingly to the increase of barrier to the tunnel electron transfers between nanocrystals. After removal of hydrogen, the film resistance returns to its initial value within 30–60 sec (Figure 2.15) so such films can be used as a reversible sensor on hydrogen.

It should be noted that the influence of hydrogen on the resistance of Pd–PPX films depends on voltage (Figure 2.16). The tunnel conductivity of initial film in the absence of hydrogen has the linear current–voltage relationship; but under the action of hydrogen, this relationship gets strongly nonlinear character and follows the equation $\ln I \sim U^{1/2}$ (see above). Hydrogen penetrating in the film disrupts the ways of tunnel current of initial film. At the same time, it is known that the absorption of hydrogen by Pd particles leads to a distortion of the Pd lattice and can give essential surface roughness of particles. As a result, the electric field between nanoparticles can rise very strongly, exceeding by several orders of magnitude the average intensity of a field in the film. This leads to an increase in the field effect on the tunnel conductivity and to the appearance of new ways for tunnel current. Therefore, as can be seen in Figure 2.16, at rather low voltages the decrease in conductivity following the action of hydrogen is replaced by an increase in conductivity.

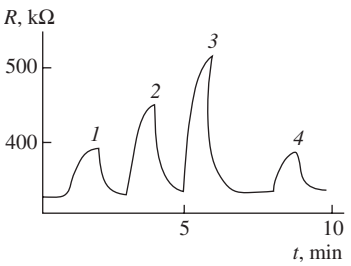


Figure 2.15. Time evolution of the resistance (*R*) of the PPX–Pd films brought into contact with hydrogen at various pressures (mm Hg): 1, 0.1; 2, 0.25; 3, 10; 4, 0.1.

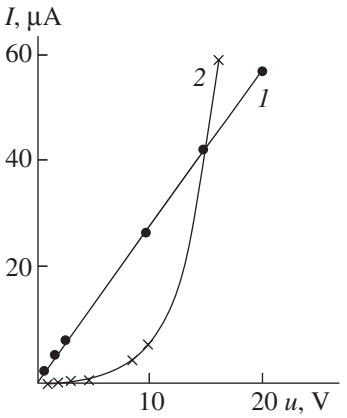


Figure 2.16. Current (*I*) versus voltage (*U*) at ambient temperature for PPX with Pd nanocrystals: 1, in pure air; 2, in hydrogen at 1 atmosphere.

## 4.3. Ferromagnetic Properties. Data Storage

The films with a high concentration of ferromagnetic nanoparticles have an application in new high-density magnetic data processing systems. Features of ferromagnetic materials consisting of domains determine magnetic data recording, each characterized by a certain direction of magnetic momentum. In the absence of an external magnetic field the magnetic moments of all domains are chaotic and the resultant moment of the ferromagnetic material is zero. With externally applied local magnetic field, the magnetic moments of domains in this area become ordered and aligned along the field, thus magnetizing the material. Such a system response is indeed a form of information recording since the direction of domain momentum is retained after the magnetic field has been removed. In this case the limiting recording density is determined, to a first approximation, by the size of domains. However, in conventional ferromagnetic materials, which are employed in magnetic hard disks, the domains interact with each other, thus limiting the density attainable for a given material size. Specialists from Seagate (a high-technology firm) have indicated that conventional magnetic disks will reach the limiting density of $2 \times 10^{10}$ bit/in.$^2$ in the near future.

In polymer composite materials, ferromagnetic nanoparticles constitute monodomains isolated in the nonmagnetic polymer matrix. In such materials the magnetic moments of nanoparticles do not interact with each other, because electron exchange between ferromagnetic particles is insignificant at interparticle distances larger than 1 nm. Therefore, each nanoparticle can be considered as one information bit, which is in the 0 or 1 logic state depending on the direc-

tion of magnetic moment relative to the direction of the external magnetic field. In metal–polymer films prepared by vapor-deposition solid-state synthesis with high composition of ferromagnetic nanoparticles, the density of the data recording has the potential to increase significantly. It has been estimated that the density of films with nanoparticles of about 5-nm size and approximately 5-nm spacing can reach about $10^{13}$ bit/in.$^2$ [4]. Such films can be used for writing, reading, and storage of the information.

The recorded information can be read by invoking the effect of negative magnetoresistance, which is the diminution of electrical resistance of the material in a magnetic field. This effect has been observed in various nanocomposite materials containing magnetic nanocrystals in a matrix of nonmagnetic metal or dielectric [67, 68]. Magnet moments of nanocrystals were oriented by a strong magnetic field. Negative magnetoresistance of composite films with ferromagnetic nanoparticles incorporated in dielectric matrix is caused by the fact that the probability of the tunnel electron transfer between neighboring nanoparticles increases if these nanoparticles have parallel orientation of spin magnet moments [69].

The phenomenon of the negative magnetoresistance has been observed recently in PPX composite films containing partially oxidized ferromagnetic Fe nanoparticles [4]. The relative change of conductivity in a magnetic field with $H = 11$ kOe is 34% at voltage around 30 V [4]. After removal of the magnetic field, the film conductivity returns to its original value; that is, the effect of magnetic field on conductivity is reversible. Total oxidation of Fe nanoparticles destroys the effect. Specific negative magnetoresistance in synthesized films containing heterogeneous nanoparticles (oxide phase around core of Fe) is not explained now. It is believed that this effect is due to interaction of magnet and dipole moments of such nanoparticles.

## 4.4. Dielectric Properties

Films of pure PPX and of PPX composites resulting from cryochemical solid-state synthesis were studied by the dielectric spectroscopy method [70]. Dielectric spectroscopy has proven very useful for studying the structure and dynamics of polymer materials, as well as the transport mechanism of charge carriers. In order to study features of the polymer structure, dielectric test methods were used because of their high sensitivity to morphological changes.

The typical three-dimensional plot of the imaginary ($\varepsilon''$) part of the complex dielectric function, $\varepsilon^*(\omega) = \varepsilon' - i\varepsilon''$, versus frequency and temperature is displayed in Figure 2.17 for the PPX composite film with 8 vol. % of Cu. The complex dielectric behavior of the dielectric losses can be described in terms of several distributed relaxation processes with some common features for all the samples. The $\varepsilon''(f, T)$ cuts at a constant frequency plane (1 kHz) for pure

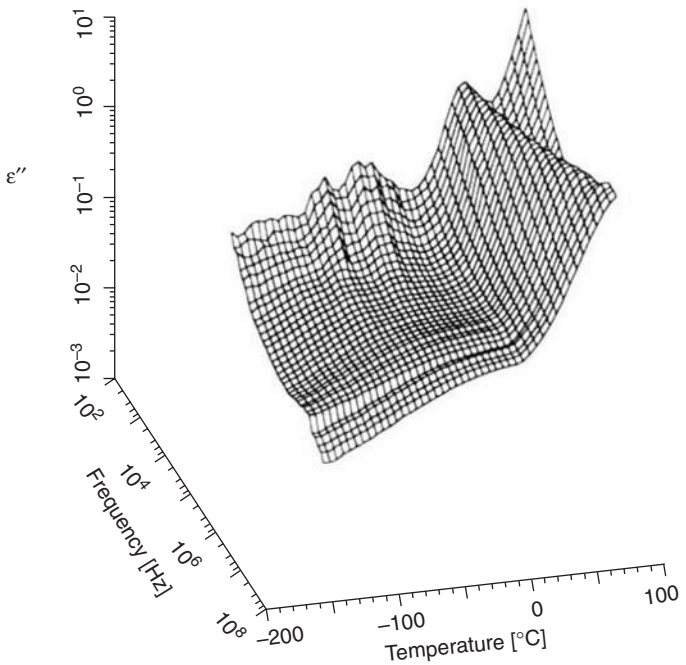


Figure 2.17. Three-dimensional plot of the frequency and temperature dependence of the dielectric losses ε″ for the sample PPX + Cu, 8 vol. %. The accuracy of the measured dielectric losses is estimated to be better than 3%.

matrix PPX and polymer matrix PPX with the addition of Cu (8 vol. %) and Zn (8 vol. %) represent the temperature dependence of the dielectric losses (Figure 2.18). A constant frequency of 1 kHz is chosen because this frequency shows all relaxation transitions.

In the temperature interval of −70 to 0°C and in the low-frequency range, an unexpected dielectric relaxation process for polymers is detected. This process is observed clearly in the sample PPX + Cu. In the sample PPX + Zn, only traces of this process can be observed, and in PPX + PbS as well as in a pure PPX matrix the process completely vanishes. The amplitude of this process essentially decreases when the frequency increases, and the maximum of dielectric losses have almost no temperature dependence. This is a typical dielectric response for percolation behavior [71, 72]. This process may relate to electron transfer between the metal nanoparticles through the polymer matrix. Data on electrical conductivity of metal-containing PPX films (see above) show that at metal concentrations higher than 5 vol. % there is an essential probability for electron transfer from one particle to another and thus such particles become involved in the percolation process.

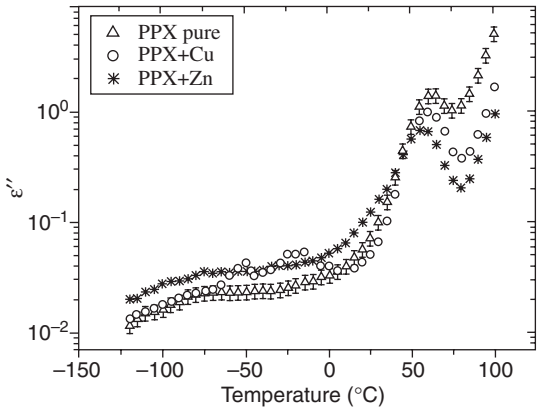


Figure 2.18. Temperature dependence of the 1-kHz frequency behavior of the dielectric losses ε″ of samples of pure PPX (Δ), PPX + Cu, 8 vol. % (○), and PPX + Zn, 8 vol. % (*).

Analysis of dielectric relaxation parameters of this process allowed us to determine the fractal properties of the percolation cluster [70]. The dielectric response for this process in the time domain can be described by the Kohlrausch–Williams–Watts (KWW) expression

$$\Psi(t/\tau) \sim \exp\left[(t/\tau)^{\nu}\right]$$

where Ψ is the dipole correlation function, τ is the average relaxation time, and ν is the stretched parameter, $0 < \nu \leq 1$. It was shown [73] that in complex fractal systems, for the relaxation caused by the charge transfer along the ramified path, the stretched parameter ν could be related to the fractal dimension $D_f$ of the percolation cluster,

$$\nu = D_f/3$$

For the sample PPX + Cu the calculated fractal dimension $D_f$ is equal to 2.609 [70]. It should be noted that the above-mentioned size distribution of metal nanoparticles leads to the mutual charging of such particles in the percolation cluster. This effect is discussed in the following section in connection with catalysis by nanoparticles. As stated in reference 70, the specific low-temperature peak of dielectric losses in the synthesized composite samples PPX + Cu is probably due to the interaction of electromagnetic field with mutually charged Cu nanoparticles immobilized in the PPX matrix. The minor appearance of this peak in PPX + Zn can be explained by oxidation of Zn nanoparticles.

The next relaxation process is typical for amorphous polymers and can be assigned to the α-relaxation that appears in the whole frequency range and in the temperature interval from 50°C to 100°C (Figures 2.17 and 2.18). This process is well-observed for all samples. It corresponds to the glass–rubber transition of the amorphous phase.

The peak of the dielectric loss of this process reflects its viscoelastic nature by obeying the time–temperature superposition principle, wherein the peak is shifted to higher temperatures for shorter times (higher frequencies) and vice versa. This process has been described by the Havriliak–Negami empirical formula [74]

$$\varepsilon^*(\omega) \sim \Delta\varepsilon \Big/ \left[1 + (i\omega\tau')^{\alpha}\right]^{\beta}$$

Here $\Delta\varepsilon$ is the dielectric strength and $\tau'$ the mean relaxation time. The parameters $\alpha$ and $\beta$ describe the symmetric and asymmetric broadening of the relaxation process. The temperature dependencies of the relaxation times of the observed α-relaxation process for pure PPX, PPX + Cu, and PPX + Zn samples demonstrate an Arrhenius behavior with the energies of activation 196 kJ/mol, 187 kJ/mol, and 201 kJ/mol, respectively, and correlate with the activation energies of the α-process in most known polymer materials [75].

## 4.5. Catalytic Activity

The adsorption of chemical compounds on nanoparticles of synthesized composites not only leads to electrical sensor effects, but also can result in new catalytic processes caused by the surface properties of such nanoparticles [61]. The important catalytic properties of PPX–metal composites prepared via cryochemical vapor deposition synthesis were discovered while studying the isomerization of 3,4-dichlorobutene into *trans*- and *cis*-1,4-dichlorobutene catalyzed by Pd nanoparticles of Pd–PPX [64] and the reaction C–Cl bonds metathesis in the mixture of *n*-decane with $CCl_4$ catalyzed by Cu nanoparticles of Cu–PPX [76].

Catalytic isomerization of 3,4-dichlorobutene was studied at 100°C in toluene. The ratio of *trans*- to *cis*-1,4-dichlorobutene for the reaction with the usual palladium catalyst is about 10. The same result was obtained by catalytic isomerization on Pd–PPX with low concentration of Pd nanoparticles. But the selectivity of the reaction decreases with increasing Pd concentration: The yield of *trans*-l,4-dichlorobutene decreases while the yield of *cis*-l,4-dichlorobutene remains constant. This result shows that the change in the catalytic properties of the composite is determined by interactions between nanoparticles rather than by the size effects. During catalytic reaction under the influence of Pd–PPX films, where the volume content of Pd nanoparticles is close to the percolation

threshold, the *trans*-to-*cis* ratio for produced isomers of l,4-dichlorobutene is about 2.9—that is, close to equilibrium value of this ratio.

Specific catalytic properties of synthesized Pd–PPX nanocomposites have been explained by charge transfer between nanoparticles at metal concentrations close to percolation threshold, when distances between nanoparticles decrease up to several nanometers and electrons can tunnel from one nanoparticle to another [59]. The effect of distances between nanoparticles on their catalytic properties has been observed at studies of oxidation of CO by Pd particles (2.8–13 nm) immobilized on the surface of MgO [77]. Nanoparticles immobilized in polymer matrix have rather wide size distribution (see above). At the same time, the energy of the Fermi level of a small metal particle depends strongly on its size and form [8, 78]. Electron transfer between particles of different size results in their mutual charging that leads to equalization of their electrochemical potentials [78]. The charging of metal nanoparticles should greatly affect catalytic reaction. In particular, the isomerization of 3,4-dichlorobutene on positively charged Pd nanoparticles proceeds, most probably, via intermediate carbonium ions to give the mixture of l,4-dichlorobutene isomers close to the equilibrium mixture [64].

Catalytic reaction of the C–Cl bonds' metathesis under the influence of a Cu–PPX nanocomposite film was studied in the mixture of *n*-decane with $CCl_4$ at molar ratio $CCl_4$/*n*-decane = 4 : 1:

$$CCl_4 + C_{10}H_{22} = CHCl_3 + C_{10}H_{21}Cl \qquad (1)$$

The reaction was conducted in the absence of oxygen at 180°C for 4 hr. The data on the yield of chlorodecanes are presented in Table 2.2 along with values of specific catalytic activity, which is defined as the number of molecules of chlorodecanes produced per Cu atom of the nanocomposite film during 1 hr of

TABLE 2.2. Dependence of Conductivity and Catalytic Activity of Nanocomposites Cu–PPX on Cu Content

| Content of Cu (vol. %) | Electrical Resistance at 77 K (Ω) | Electrical Resistance at 298 K (Ω) | Yield of Chlorodecanes (mol. %) | Specific Catalytic Activity |
|---|---|---|---|---|
| 1.3 | ∞ | ∞ | Traces | Traces |
| 3.5 | $7.0 \times 10^8$ | $3.5 \times 10^8$ | 4 | 130 |
| 5.0 | $10.2 \times 10^3$ | $8.3 \times 10^3$ | 15 | 500 |
| 7.0 | $3.3 \times 10^3$ | 645 | 20 | 650 |
| 10.3 | 66 | 29 | 35 | 1150 |
| 14 | $16.2 \times 10^3$ | $3.1 \times 10^3$ | 14 | 450 |

the reaction. The data on the reaction are related to the data on the electrical resistance ($R$) of the composite films.

At very small concentration of Cu ($X_{cu}$) around 1 vol. %, the $R$ value of the composite film is close to that of pure PPX. In this case, Cu nanoparticles fully isolated in matrix do not interact with one another and do not influence the composite conductivity. But is seen in the table, the increase of $X_{Cu}$ even to 3.5 vol. % leads to the sharp fall of $R$ as a result of charge transfer between Cu nanoparticles. The probability of such transfer rises exponentially with the decrease of distance between particles—that is, with $X_{Cu}$ increasing.

At the same time, the lowering of $R$ with temperature in the range from 77 to 298 K indicates that even at the maximal Cu concentration investigated, the composite film is the system of metal "islands" in dielectric matrix. The true percolation threshold [59], at which the film shows the metallic behavior characterized by the increase of $R$ with temperature, is not achieved. At the same time, the data on $R$ (Table 2.2) suggest that at $X_{Cu}$ in the range 5–10 vol. % the obtained Cu-nanoparticle ensemble in the PPX matrix is close to the percolation threshold. But the further increase of $X_{Cu}$ up to 14% gives rise to explosive aggregation of nanoparticles with formation of isolated large-scale metal inclusions: This process is accompanied by the substantial decrease in the number of metal nanoparticles and the corresponding rise of $R$ (Table 2.2).

At very low $X_{Cu}$, the catalytic activity of fully isolated and noninteracting Cu nanoparticles in PPX (see Table 2.2) is very small. The increase of $X_{Cu}$ leads to the strong gain in catalytic activity, which achieves the maximum near the percolation threshold under the conditions of the most effective interaction between metal nanoparticles isolated in the polymer matrix. The metal aggregation of metal nanoparticles results in the fall of the catalytic activity. The maximal specific activity is 1150, which is much greater than the activity of all known catalysts in this reaction. For comparison, the same reaction of C–Cl bond metathesis was investigated on the special prepared catalyst containing 1 mass % of high dispersed metallic Cu deposited on silica. In conditions analogous to those of the reaction on the nanocomposite Cu–PPX film, the specific activity of this catalyst is 4. Moreover, it has low selectivity: In this case the formation of by-products from condensation processes accompanies the reaction, whereas the Cu–PPX catalyst gives monochlorosubstituted decanes only.

The initiation of the reaction (1) is carried out as a result of dissociation C–Cl bonds with formation of initiating radicals $CCl_3$:

$$CCl_4 \rightarrow CCl_3 + Cl \tag{2}$$

The energy expenditure of this reaction in gaseous phase ($E_i^v$) differs from that of the same reaction in the adsorption state on Cu ($E_i^{ad}$) by the value $E_i^{ad} - E_i^v = Q^{ad}(Cl) + Q^{ad}(CCl_3) - Q^{ad}(CCl_4)$, where $Q^{ad}(X)$ is the heat of adsorption of

corresponding molecule. Most likely the heat of adsorption of $CCl_4$ on Cu is less than that of adsorption of Cl or radical $CCl_3$, so that $E_i^{ad} - E_i^{v} > 0$, and the adsorption of $CCl_4$ on Cu particles should favor its dissociation and initiation of reaction. But obtained data (Table 2.2) lead to the conclusion that this effect is rather insignificant at very low metal content, when isolated Cu particles in PPX are located far apart so the charge transfer between particles is practically impossible and they remain neutral. The increase of reactivity with the rise of metal content can be explained by the mutual charging of Cu nanoparticles. Presumably, negatively charged particles formed in this case, among positively charged ones, facilitate the process of initiation. Because $CCl_4$, $CCl_3$, and Cl have the significant electron affinity ($E_A$ is about 2 eV for $CCl_4$, 1.5 eV for $CCl_3$, and 3.6 eV for Cl), $Q^{ad}$ should increase due to the very great $E_A$ of Cl atom. Consequently, one would expect the increase of the rate of $CCl_4$ dissociation.

The effect of charge on the dissociation of $CCl_4$ should be especially strong on roughness of the nanoparticle surface where the electron work function decreases because of the sharp increase of the charge density on such roughness. In this connection, it should be noted that nanoparticles have the high percentage of atoms on or near the surface (for example, a 5-nm CdS-particle has about 15% of the atoms on its surface) [61]. The structure and properties of such vast interface between the particle and surrounding medium depend, to a large measure, on this medium. Unlike nanoparticles formed in the gaseous phase and characterized by a quasi-equilibrium surface, which is nearly the same as that of bulk metal, nanoparticles produced and immobilized in a solid or highly viscous matrix can have the defect rough surface, because of hindering formation of equilibrium surface structure from matrix. As a result, catalytic properties of such nanoparticles can be greatly influenced by a polymer matrix (cf. reference 79).

## 5. CONCLUSIONS

The cryochemical vapor deposition synthesis of metal–polymer films (from the gaseous state to the solid polymer one, bypassing the liquid phase) allows the production of both new organometallic structures and new valuable composites with high concentrations of nano-sized metal or semiconductor particles.

Solid-state synthesis of this type draws the special attention in connection with an opportunity to prepare and stabilize small clusters of metal or semiconductor atoms in a polymeric matrix at ambient and even higher temperatures. Size-dependent quantum states in such clusters, which are the intermediate form between metal atoms and bulk metal, can give new electronic, optical, and magnetic effects [80]. The structure and properties of clus-

ters in synthesized polymer systems are still almost unknown. The study of clusters in the rather wide (up to 300–320 K) temperature range and in various polymer matrices can give insight into important basic and applied problems of cluster science.

The cluster aggregation at heating of cryochemically synthesized systems gives polymer composites containing metal or semiconductor nanocrystals. The composites prepared in this manner, unlike other analogous materials, demonstrate a marked increase in the percentage of small crystals with increasing content of inorganic component (metal or semiconductor) incorporated in a polymer, although the mean size of nanocrystals thus remains practically constant. It should be noted that the effect of the metal particle size on the energy of Fermi level and work function of a particle becomes appreciable for nanoparticles of size less than 5 nm [8]. Correspondingly, the mutual charging of metal inclusions in a polymer composite can significantly affect physical and chemical properties of composite if the concentration of such nanoparticles is great enough to provide tunnel electron transfer between them in all volume of a composite, because it takes place in the synthesized composites, where they are the main part of total number of particles even at high metal content.

The technique of the low-temperature solid-state polymerization of the vapor-deposited metal (or semiconductor)–monomer co-condensates provides a possibility to vary the structure of a polymer matrix in a rather wide range. In this connection, it should be noted that not only *p*-xylylene and its derivatives containing various substituents including strong polar ones [24, 44], but also other monomers (e.g., reference 18), can be used as initial compounds. Although the study of the cryochemical solid-state synthesis, as well as structure and properties of obtained materials, is only in an initial stage, now it is clear that this synthesis gives much promise for producing new intriguing metal-containing polymers that can be of great importance in various fields of science and technique.

## REFERENCES

1. D. Woehrle, in *Macromolecule–Metal Complexes*, edited by F. Ciardelli, E. Tsushida, D. Woehrle, Springer-Verlag, Berlin, (1996), p. 100.
2. A. D. Pomogailo, A. S. Rozenberg, I. Ye. Uflyand, *Nanoparticles of Metals in Polymers*, Chemistry Moscow (2000), pp. 1–673.
3. M. P. Andrews and G. A. Ozin, *Chem. Mater.* **1**, 174 (1989).
4. L. I. Trakhtenberg, G. N. Gerasimov, and E. I. Grigoriev, *Russian J. Phys. Chem.* **73**, 209 (1999).
5. K. J. Klabunde, *Free Atoms, Clusters and Nanoscale Particles*, Academic Press, San Diego (1994), p. 311.

6. M. Ritala, K. Kukli, A. Rahtu, P. I. Raisanen, M. Leskela, T. Sajavaara, and J. Keinonen, *Science* **288**, 319 (2000).
7. M. Moskovits, in *Cryochemistry*, edited by G. A. Ozin, John Wiley & Sons, New York, (1976), pp. 1–594.
8. E. Shumacher, *Chimia* **42**, 357 (1988).
9. M. P. Andrews and G. A. Ozin, *J. Phys. Chem.* **90**, 2922 (1986).
10. M. A. Petrukhina, L. N. Alexandrova, V. V. Zagorskii, G. B. Sergeev, I. E. Kardash, and G. N. Gerasimov, *Proceedings of Fifth Soviet Union Conference on Low Temperature Chemistry*, December 10–13, 1991, Moscow University, Moscow (1991), p. 130.
11. R. W. Zoelner and K. J. Klabunde, *Inorg. Chem.*, **23**, 3241 (1984).
12. V. A. Sochilin, I. E. Kardash, and G. N. Gerasimov, *Polym. Sci. (Russia)* **37**, 1938 (1995).
13. G. Gardenas T., K. J. Klabunde, and H. Habdas, *Chem. Mater.* **1**, 481 (1989).
14. G. Gárdenas T., C. Retamal C., and K. J. Klabunde, *J. Appl. Polym. Sci.* **49**, 15 (1991).
15. G. Gárdenas T., C. Retamal C., and K. J. Klabunde, *Polym. Bull. (Berlin)* **25**, 315 (1991).
16. G. Gárdenas T. and C. Muñoz D., *Makromol. Chem.* **194**, 3377 (1993).
17. V. A. Kabanov, G. B. Sergeev, V. P. Zubov, and V. A. Kargin, *Vysokomol. Soed. (Polym. Sci.)* **1**, 859 (1959).
18. G. N. Gerasimov, S. M. Dolotov, and A. D. Abkin, *Radiat. Phys. Chem.* **15**, 405 (1980).
19. C. Chachaty and M. Magat, *J. Polymer Sci.* **48**, 139 (1960).
20. G. N. Gerasimov and A. D. Abkin, *Khim. Fiz.* (*Chem. Phys. Rep.*) **3**, 170 (1984).
21. E. S. Mansueto and Ch. A. Wight, *J. Am. Chem. Soc.* **111**, 1900 (1989).
22. L. M. Alexandrova, L. V. Shundina, G. N. Gerasimov, and I. Ye. Kardash, *Polym. Sci. (Russia)* **35**, 361 (1993).
23. L. N. Alexandrova, V. A. Sochilin, G. N. Gerasimov, and I. E. Kardash, *POLIMEX-93 International Symposium on Polymers*, November, 1993, Cancun, Mexico, Preprints, p. 150.
24. G. N. Gerasimov, V. A. Sochilin, S. N. Chvalun, L. V. Volkova, and I. Ye. Kardash, *Macromol. Chem. Phys.* **197**, 1387 (1996).
25. N. N. Semenov, *J. Polym. Sci*. **55**, 563 (1961).
26. V. I. Goldanskii, *Nature* **279**, 109 (1979).
27. S. F. Timashov and L. I. Trakhtenberg, *Russ. J. Phys. Chem.* **67**, 209 (1993).
28. M. V. Basilevsky, G. N. Gerasimov, S. I. Petrochenko, and V. A. Tikhomirov, *Chem. Phys*. **55**, 259 (1981).
29. L. Alexandrova and R. Vera-Graziano, in J. C. Salamone, ed., *Polymeric Materials Encyclopedia*, Vol. 9, CRC Press, Boca Raton, FL (1996), p. 7180.
30. G. N. Gerasimov, E. I. Grigoriev, A. E. Grigoriev, P. S. Vorontsov, S. A. Zavialov, and L. I. Trakhtenberg, *Chem. Phys. Rep.* **17**, 1247 (1998).

31. E. Kay, *Z. Phys. D—Atoms, Molecules and Clusters* **3**, 251 (1986).
32. H. Hopf, G. N. Gerasimov, S. N. Chvalun, V. I. Rosenberg, E. L. Popova, E. V. Nikolaena, E. I. Grigoriev, L. I. Trakhtenberg, and S. A. Zavyalov, *Adv. Mater. Chem. Vap. Depos.* **3**, 197, (1997).
33. G. N. Gerasimov, E. L. Popova, E. V. Nikolaeva, S. N. Chvalun, E. I. Grigoriev, L. I. Trakhtenberg, V. I. Rosenberg, and H. Hopf, *Macromol. Chem. Phys.* **199**, 2179 (1998).
34. G. Sergeev, V. Zagorsky, and M. Petrukhina, *J. Mater. Chem.* **5**, 31 (1995).
35. L. N. Alexandrova, V. A. Sochilin, G. N. Gerasimov, and I. E. Kardash, *Polymer* **38**, 721 (1997).
36. L. Alexandrova, E. Sansores, E. Martinez, E. Rodrigez, and G. Gerasimov, *Polymer* **42**, 273 (2001).
37. L. I. Trakhtenberg, G. N. Gerasimov, L. N. Aleksandrova, and V. K. Potapov, *Radiat. Phys. Chem.* **65**, 479 (2002).
38. A. A. Arest-Yakubovich, R. V. Basova, and E. A. Birman, *Vysokomol. Soed. (Polym. Sci.)* **B21**, 226 (1979).
39. H. F. Ebel and B. O. Wagner, *Chem. Ber.* **104**, 307 (1971).
40. E. Weiss, *J. Organomet. Chem.* **2**, 314 (1964).
41. E. Weiss, *J. Organomet. Chem.* **4**, 101 (1965).
42. L. Alexandrova, D. Likhachev, S. Muhl, R. Salcedo, G. Gerasimov, and I. Kardash, *J. Inorg. Organomet. Polym.* **8**, 157 (1998).
43. L. I. Trakhtenberg, G. N. Gerasimov, E. I. Grigoriev, A. E. Grigoriev, I. E. Kardash, S. V. Radzig, P. S. Vorontsov, and S. A. Zavialov, *Proceedings of Second International Conference on Low Temperature Chemistry*, edited by J. R. Durig and K. J. Klabunde, Bk Mk Press, Kansas (1996), p. 211.
44. G. N. Gerasimov, E. V. Nikolaeva, E. I. Smirnova, V. A. Sochilin, and L. I. Trakhtenberg, *Doklady Phys. Chem.* **380**, 184 (2001).
45. A. W. Olsen and Z. H. Kafafi, *J. Am. Chem. Soc.* **113**, 7758 (1993).
46. G. B. Sergeev, *Nanochemistry*, Moscow University, Moscow, 2003, p. 85.
47. K. P. Charle, F. Frank, and W. Schulze, *Ber. Bunsenges. Phys. Chem.* **88**, 350 (1984).
48. C. Carotenuto, G. P. Pepe, and L. Nicolais, *Eur. Phys. J.* **B16**, 11 (2000).
49. U. Kreibig and C. von Fragstein, *Z. Phys.* **224**, 307 (1969).
50. L. Genzel, T. P. Martin, and U. Kreibig, *Z. Phys.* **B21**, 339 (1975).
51. P. Apell and Å. Ljungbert, *Solid State Commun*. **44**, 1367 (1982).
52. G. B. Bushueva, V. V. Zagorskii, G. M. Zinenkova, M. A. Petrukhina, O. V. Revokatov, and G. B. Sergeev, *Russ. Phys. Bull.* **61**, 1871 (1997).
53. E. V. Nikolaeva, S. A. Ozerin, A. E. Grigor'ev, E. I. Grigor'ev, S. N. Chvalun, G. N. Gerasimov, and L. I. Trakhtenberg, *Mater. Sci. Eng.* **C8–9**, 217 (1999).
54. L. I. Trakhtenberg, A. B. Rabinovich, V. A. Kaminskii, and G. N. Gerasimov, *Chem. Phys. Rep.* **21**, 69 (2002).

55. O. J. Ilegbusi, M. Iguchi, and W. Wahnsiedler, *Mathematical and Physical Modeling of Materials Processing Operations*, Chapman & Hall/CRC, New York (1999).
56. E. V. Nikolaeva, Ph.D. Thesis, Karpov Institute of Physical Chemistry, Moscow, 1999.
57. S. A. Ozerin, M.D. Thesis, Moscow Physical Technical Institute, Moscow, 1999.
58. L. I. Trakhtenberg, Yu. F. Krupyanskii, and G. N. Gerasimov, *Chem. Phys. Rep.* (in press).
59. D. Yu. Godovski, *Adv. Polym. Sci.* **119**, 58 (1995).
60. J. G. Simmons, *J. Appl. Phys.* **35**, 2472 (1964).
61. Y. Wang and N. Herron, *J. Phys. Chem.* **95**, 525 (1991).
62. G. Sergeev, V. Zagorsky, M. Petrukhina, S. Zav'yalov, E. Grigor'ev, and L. Trakhtenberg, *Anal. Commun.* **34**, 113 (1997).
63. L. I. Trakhtenberg, E. Axelrod, G. N. Gerasimov, A. E. Grigoriev, E. I. Grigoriev, S. A. Zav'yalov, and Yu. Feldman, *Sci. Isr.—Technol. Adv.* **1**, 572 (1999).
64. P. S. Vorontsov, E. N. Golubeva, E. I. Grigor'ev, S. A. Zavyalov, L. M. Zavyalova, and L. I. Trakhtenberg, *Russ. J. Phys. Chem.* **72**, 1912 (1998).
65. R. M. Hill, *ERA Research Report*, No. 5232 (1967), p. 1.
66. P. D. Cobden, B. E. Nieuwenhuyas, and V. V. Gorodetskii, *Appl. Catal.* **A188**, 69 (1999).
67. T. Furubayasci and I. Nakatani, *J. Appl. Phys.* **79**, 6250 (1996).
68. L. R. Schlep, A. Fert, P. Fettar, P. Holady, S. F. Lee, J. L. Maurice, F. Petroff and A. Vaurěs, *Phys. Rev.* **B56**, 5747 (1997).
69. B. Fugimori, S. Mitani, S. Ohnuma, *J. Appl. Phys.* **79**, 4733 (1996).
70. L. I. Trakhtenberg, E. Axelrod, G. N. Gerasimov, E. V. Nikolaeva, and E. I. Smirnova, *J. Non-Cryst. Solids* **305**, 190 (2002).
71. Yu. Feldman, N. Kozlovich, I. Nir, and N. Garti, *Phys. Rev.* **E51**, 478 (1995).
72. A. Gutina, E. Axelrod, A. Puzenko, E. Rysiakiewicz-Pasek, N. Kozlovich, and Yu. Feldman, *J. Non-Cryst. Solids* **302**, 235 (1998).
73. Yu. Feldman, N. Kozlovich, Yu. Alexandrov, R. Nigmatullin, and Ya. Ryabov, *Phys. Rev.* **E54**, 5420 (1996).
74. A. Schynhals, in *Dielectric Spectroscopy of Polymeric Materials: Fundamentals and Applications*, edited by James P. Runt, John J. Fitzgerald, American Chemical Society, Washington, DC (1997), pp. 81–106.
75. S. Havriliak and S. Negami, *Polymer* **8**, 161 (1967).
76. L. I. Trakhtenberg, G. N. Gerasimov, E. I. Grigoriev, S. A. Zav'yalov, O. V. Zagorskaya, V. Yu. Zufman, and V. V. Smirnov, in *Studies in Surface Science and Catalysis,* Vol. 130, 12th ICC, Part B, edited by A. Corma, F. V. Melo, S. Mendioroz and J. L. G. Fierro, Elsevier, Amsterdam (2000), p. 941.
77. C. Becker and C. R. Henry, *Surf. Sci.* **352–354**, 457 (1996).
78. E. L. Nagaev, *Phys. Usp.* **162**, 49 (1992).
79. M. C. M. Alves, and G. Tourillon, *J. Phys. Chem.* **100**, 7566 (1996).
80. J. I. Brauman, *Science* **271**, 889 (1996).